Lawrence Berkeley Laboratory
UNIVERSITY OF CALIFORNIA

Materials & Molecular Research Division

Submitted to the Journal of Applied Physics

THERMAL GRADIENT MIGRATION OF BRINE INCLUSIONS IN SYNTHETIC ALKALI HALIDE SINGLE CRYSTALS

D.R. Olander, A.J. Machiels, M. Balooch, and S. Yagnik

January 1981

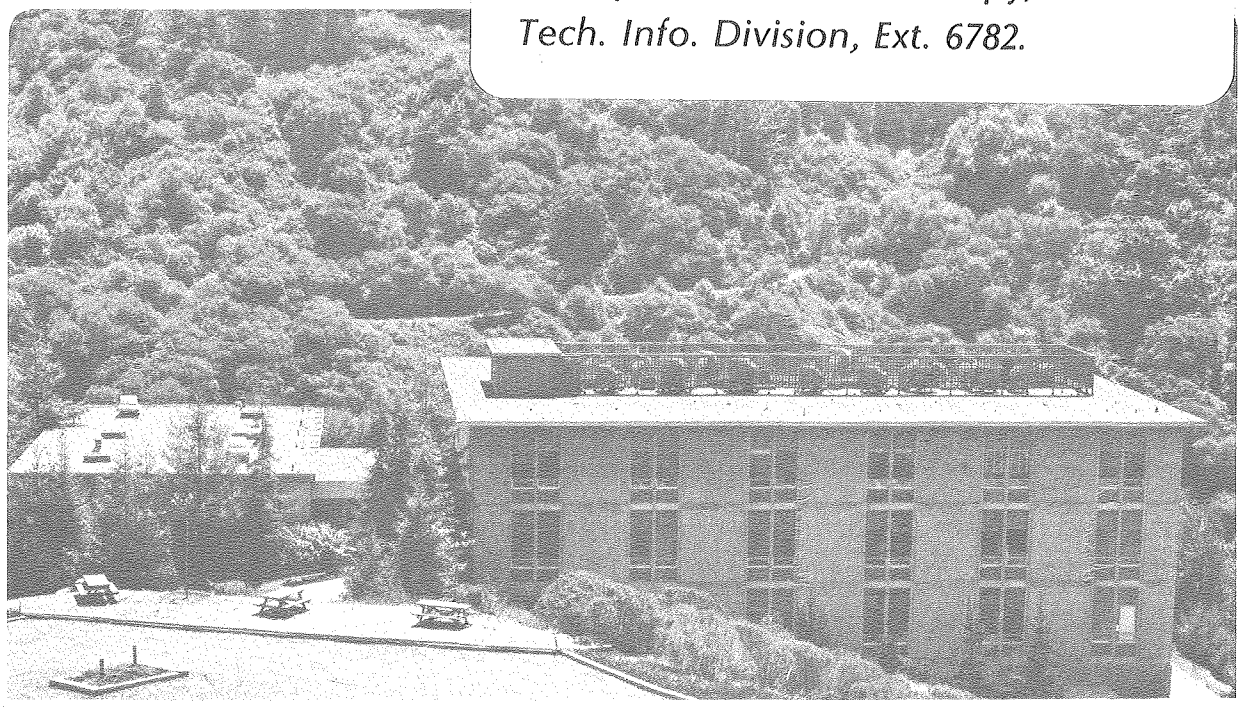

Prepared for the U.S. Department of Energy under Contract W-7405-ENG-48

DISCLAIMER

LBL-12163

THERMAL GRADIENT MIGRATION OF BRINE INCLUSIONS IN SYNTHETIC ALKALI HALIDE SINGLE CRYSTALS

by D. R. Olander
A. J. Machiels
M. Balooch
S. Yagnik

Materials and Molecular Research
Division of the Lawrence Berkeley
Laboratory and the
Department of Nuclear Engineering
University of California, Berkeley
Berkeley, California 94720

*present address: Nuclear Engineering Program, University of Illinois, Urbana, Illinois

This work was supported by the Director, Office of Energy Research, Office of Basic Energy Sciences, Materials Sciences Division of the U.S. Department of Energy under contract # W-7405-ENG-48 and by the Office of Nuclear Waste Isolation.

ABSTRACT

An apparatus consisting of an optical microscope with a hot stage attachment capable of simultaneously non-uniformly heating and mechanically loading small single crystals of salt was used to measure the velocities of all-liquid inclusions in NaCl and KCl specimens under various conditions of temperature, temperature gradient, and uniaxial stress. The rate-controlling elementary step in the migration of the inclusions was found to be associated with interfacial processes, probably dissolution of the hot face. Dislocations are required for this step to take place. The small number of dislocation intersections with small inclusions in nearly perfect crystals causes substantial variations in the velocity, a sensitivity of the velocity to mechanical loading of the crystal, and a velocity which varies approximately as the square of the temperature gradient.

INTRODUCTION

Natural salt deposits contain small inclusions of brine distributed as small intragranular inclusions and as water on grain boundaries. Storage of heat-generating nuclear wastes in the salt causes both types of water to migrate up the temperature gradient towards the heat source. The resulting accumulation of brine around the waste package can contribute to corrosion of the metallic canister and to leaching of the glass or ceramic wasteform which contains the fission products and heavy metals. Grain boundaries in polycrystalline rock salt are apparently quite weak and open up due to the thermal stresses which accompany the thermal gradients,

allowing water contained in the grain boundaries to be released by a vapor transport process(1). Upon reaching a grain boundary, intragranular inclusions lose most of their liquid, which also escapes by evaporation(2). However, intragranular water must first be transported to the grain boundaries to escape. With a typical grain size of 1 cm, the latter step may control the rate of water loss from rock salt surrounding a waste canister. Consequently, understanding of the mechanism of inclusion mobility in salt crystals is important for the evaluation of bedded or dome salt as possible geologic media for nuclear waste repositories.

Present models used to predict brine inclusion migration in rock salt make extensive use of the results of Anthony and Cline(3) and Geguzin et al(4). Their measurements, however, were obtained with KCl, not NaCl, in a very narrow range of temperatures. Therefore, a more extensive experimental investigation of the migration velocities of brine inclusions in synthetic single crystals of NaCl and KCl has been conducted.

The intragranular brine contained within the salt crystals migrates in the temperature gradient by the same mechanism by which pores move in nuclear fuels, namely by diffusional transport of the dissolved salt from the hot face of the cavity to the cold face. The solubility of salt in brine increases with temperature, so in a temperature gradient salt dissolves into the inclusion at the hot surface and crystallizes out at the cold surface. Transport occurs by thermal and molecular diffusion of salt within the liquid phase. The salt flux through the liquid from the hot to the cold

faces causes the inclusion to move in the opposite direction. However, kinetic resistances to dissolution and crystallization rather than transport in the liquid control the migration velocity in KCl. Evidence of rate-limiting dissolution and crystallization steps suggests that the migration process may be dependent upon defects in the solid, in particular its dislocation density. Therefore, in addition to controlling the temperature and temperature gradient in the experiments, a means of varying the mechanical load on the crystal specimens was also developed.

EXPERIMENTAL

The experimental setup used to study the behavior of brine inclusions in salt single crystals shown in Fig. 1 is a transmitted-light microscope equipped with a hot stage attachment which maintains the temperature profile in the salt while applying a constant uniaxial stress to the specimen. The hot stage attachment consists of two rectangular copper blocks A and B fixed to insulator plate C. The copper blocks are heated externally by heaters D and E and clamp the salt crystal F between the end faces, which have been polished and gold-plated to promote good thermal contact. The temperatures close to the crystal end faces are measured by thermocouples T1 and T2. In a special test, the ability to infer the temperature distribution within the crystal using these two external thermocouples was verified. Three holes were drilled along the length of a crystal into which thermocouples were inserted and fixed by conducting epoxy. The measured temperature distribution in the crystal was found to be in excellent agreement with

the expected linear profile joining the external temperatures measured by T1 and T2.

Block B is actually a hollow shell with two sliding copper pieces G and H, the movements of which are controlled by knob I. A miniature load cell J is placed between G and H and the axial load on the specimen is measured by the transducer of the load cell.

Synthetic single crystals of NaCl and KCl with dimensions of 15 mm x 5 mm x 5 mm with (100) end faces were obtained from the Harshaw Chemical Co. The dislocation densities in the crystals were measured by developing etch pits on the surface(5 - 7). This method involves treating the surface with selected chemical etchants which produce a pit on the surface at the site of each emerging dislocation. The etch pits so formed can be counted under an optical microscope. Figure 2 shows the etch pits on a NaCl (100) surface. A typical NaCl crystal used in this investigation contains $\sim 10^5$ dislocations/cm^2. The dislocations are often observed in clusters rather than as the uniform distribution shown in Fig. 2.

Synthetic inclusions are produced in the crystal by drilling a 0.3 mm diameter hole 3 mm deep in an end face and filling the hole with deionized water. The crystal is placed between the copper blocks of the hot stage with a sheet of rubber covering the end with the hole to prevent evaporation of the water. By applying a temperature gradient of 10 - 30^{o}C per cm for several days, the water-filled cavity spawns a cloud of tiny all-liquid inclusions with a size distribution ranging from 10 to 100 μm. These

inclusions are initially cubical with (100) planes as faces. When a temperature gradient is applied in a (100) direction, the inclusions move towards the hot end and at the same time change to square disks which are flattened in the direction of the thermal gradient (Fig. 3). This shape change, which takes several hours to complete, does not alter the cavity volume. However, the final thickness of the platelet depends upon the magnitude of the applied temperature gradient. Very small inclusions (those initially less than $\sim 10\ \mu m$ on a side) do not move or change shape in the thermal gradient and very large inclusions break up into smaller ones during the initial stage of shape change. When the temperature gradient is applied in a different crystallographic direction, the shapes of the inclusions are more complicated (chevron-type) but their terminal velocities are not significantly different from those in (100) temperature gradients for the same conditions.

A typical observation consists of measuring the dimensions of the inclusion (thickness L and width W) and the distance travelled during the time between successive observations. With the setup described above, these quantities can be measured with an accuracy of $\pm$ 1 μm. To avoid errors due to thermal expansion or creep of the salt, inclusion positions are measured relative to a reference scratch on the crystal surface. Migration is reversible in the sense that changing the direction of the temperature gradient causes the inclusions to move in the opposite direction at the same speed.

When the temperature gradient is removed from inclusions which have achieved their terminal shape, relaxation towards a cube takes

place; the width decreases and the thickness increases but the aspect ratio L/W never reaches unity.

TEMPERATURE GRADIENTS IN THE INCLUSION

All theories of the migration process require knowledge of the temperature gradient in the inclusion, ∇T_ℓ, but what is established experimentally is the temperature gradient in the bulk solid, ∇T_∞. Because the brine is a poorer conductor of heat than the solid salt, ∇T_ℓ is larger than ∇T_∞. A complete temperature distribution inside the inclusion can be obtained as a function of the aspect ratio by solving Laplace's equation in both solid and liquid and using heat flux and temperature continuity conditions at the cavity boundaries. Numerical solutions obtained with the code HEATING 5 are shown in Fig. 4 in terms of a thermal gradient amplification factor defined by

$$\alpha = \frac{\nabla T_\ell}{\nabla T_\infty} \tag{1}$$

This factor is a function of the aspect ratio of the inclusion, L/W, and the off-axis position, X. On the axis of the inclusion, the amplification factor is bounded by:

$$\alpha\ (X = 0) = \begin{cases} 3/(2+k_\ell/k_s) \text{ for } L/W = 1 \\ k_s/k_\ell \text{ for } L/W = 0 \end{cases} \tag{2}$$

where k_s and k_ℓ are the thermal conductivities of the solid and liquid, respectively; their ratio is ~ 7 for NaCl and ~ 10 for KCl. The value of the amplification factor for the cubical inclusion is essentially equal to that for a sphere. The formula obtained by Stoner (8)

for prolate spheroids

$$\mathcal{A}(X = 0) = \left[(1 - F) + F(k_\ell/k_s) \right]^{-1} \tag{3}$$

where:

$$F = \frac{1}{1-(L/W)^2} \left\{ 1 - \frac{(L/W) \cos^{-1} (L/W)}{1-(L/W)^2} \right\} \tag{4}$$

has been used to represent the gradient on the axis of the square platelets(3). Note that Eqs. (3) and (4) exhibit the limiting behavior indicated by Eq. (2).

The variation of the thermal gradient amplification factor with off-axis location is just as important as its dependence upon the inclusion aspect ratio. Figure 4 shows that $\mathcal{A}$ is largest on the axis (X = 0) but decreases to unity at the edge of the inclusion (X = W/2). For example, consider an inclusion in NaCl with an aspect ratio L/W of 1/6. Figure 4 shows that the temperature gradient on the inclusion axis is $\sim$ 3 times larger than ∇T_∞, but at 1/3 of the distance between the axis and the edge (X = L), the amplification factor has been reduced to $\sim$ 2. At two thirds of the way to the edge (X = 2L), ∇T_ℓ is approximately equal to ∇T_∞. In this particular example, there is an uncertainty (or variation) of a factor of 3 in relating ∇T_ℓ to ∇T_∞. No theory of inclusion migration provides guidance on the choice of ∇T_ℓ. Yet because the inclusion retains (100) faces perpendicular to the applied temperature gradient, it is evident that only a single value of ∇T_ℓ controls the migration speed. If the kinetics of dissolution,

diffusion, and crystallization followed the local value of ∇T_ℓ, the inclusion would adopt a spherical shape. Obviously the great stability of the (100) faces prevents such deformation. As shall be seen later, the enormous scatter in the measurements of inclusion velocity under the same nominal experimental conditions observed by all investigators is in large part due to the variation of the thermal gradient across the face of the inclusion.

INCLUSION SHAPES

Application of a temperature gradient causes an inclusion to migrate and at the same time to flatten out in the direction of the gradient. Upon removal of the temperature gradient, motion ceases and the inclusion returns to a nearly cubical shape. These dimensional changes which accompany application and removal of a temperature gradient can be analyzed thermodynamically by equating the free energy change due to transfer of dissolved salt from the sides of the inclusion to the cold face to the surface work required to change the inclusion aspect ratio(3,4,9). The analysis is summarized in the Appendix and leads to a terminal thickness in a temperature gradient of:

$$L = \left[\frac{2\gamma C_s^{sat}}{\rho_s RT(dC_s^{sat}/dT)\ \nabla T_\infty}\right]^{1/2} \qquad (5)$$

where γ is the specific surface energy of the (100) faces of the alkali halide, C_s^{sat} is the solubility of the salt in water at the mean temperature T and ρ_s is the density of the solid salt. Our experiments, as well as those of Anthony and Cline(3,9) and

Geguzin et al (4) have verified the inverse square root relationship between L and ∇T_∞ and the size-independence of L implied by Eq. (5). Figure 5 shows the initial deformation process for three inclusions caused by application of a temperature gradient. For the particular gradient chosen, the terminal thickness is $\sim$ 10 μm, independent of initial size except for the smallest inclusion which is nearly immobile. The increase in the lateral dimension W of one of the inclusions which accompanies the flattening process is also shown in the graph. The inclusion volume is constant during the shape change. Figure 6 shows the variation of the terminal thickness with temperature gradient at a fixed temperature. Experiments of this type were conducted for temperatures ranging from 40°C to 125°C. These measurements permit determination of the crystal surface energy.

The same theoretical analysis can be extended to calculate the terminal shape of the relaxed inclusion after removal of the temperature gradient. The departure from a perfect cube is found to be:

$$\left(\frac{W}{L} - 1\right)_{\nabla T=0} = \frac{\rho_s RT}{2\gamma} \left(\zeta^*_{dis} + \zeta^*_{crys}\right) W \qquad (6)$$

where ζ^*_{dis} is the critical fractional undersaturation of the liquid required for dissolution of the salt and ζ^*_{crys} is the critical fractional supersaturation needed for crystal growth. Measurement of the final aspect ratio of the inclusion after removal of the temperature field permits these nucleation properties of the salt/water system to be determined.

The first two rows of table 1 compare the interfacial properties

properties of NaCl and its brine determined in the present study with the corresponding values for the KCl system obtained by Anthony and Cline (3,9) and Geguzin et al (4). At 40°C, the (100) surface energy is larger for KCl than for NaCl but the reverse is true for the critical sub- and supersaturations. The information in the last row of the table is discussed below.

Table 1

Properties of the KCl-H_2O and NaCl-H_2O Interfaces at 40°C

Parameter	Ref. 4 (KCl)	Ref. 3,9 (KCl)	This Work (NaCl)
γ, erg/cm^2	30	37	16
$\left(\zeta^*_{dis}+\zeta^*_{crys}\right) \times 10^5$	1.2	1.0	3.5
$(1/k_{dis}+1/k_{crys})^{-1} \times 10^5$, moles/cm^2-s	6	4.5	0.2-6

MIGRATION VELOCITY-LINEAR INTERFACE KINETICS

Figure 7 shows an inclusion of small aspect ratio in a temperature gradient. The symbols $\left(C_s^{sat}\right)_h$ and $\left(C_s^{sat}\right)_c$ denote the equilibrium solubilities of salt in water at the hot and cold sides of the inclusion, respectively.

Because the temperature difference across the inclusion is very small ($\sim 0.01^oC$), the difference in solubilities can be approximated by:

$$\left(C_s^{sat}\right)_h - \left(C_s^{sat}\right)_c \simeq \frac{dC_s^{sat}}{dT} L \nabla T_\ell \qquad (7)$$

The temperature gradient to use in this equation is not well defined because as shown previously, ∇T_ℓ is a function of lateral position on the inclusion. The value on the inclusion axis has been used in previous studies (3,4) and we will follow the same procedure here. The effect of this uncertainty will be discussed later.

Salt transport from the hot to the cold face of the inclusion proceeds through a three-step series mechanism:

1. dissolution at the hot face
2. ordinary and thermal diffusion through the liquid
3. crystallization at the cold face

The flux of salt for each step is denoted by j_s and the inclusion velocity is:

$$v = j_s/\rho_s \tag{8}$$

Molecular transport in the liquid by ordinary and thermal diffusion is given by:

$$j_s = \frac{D_\ell}{L}\left(C_s^h - C_s^c\right) - \sigma D_\ell C_s^{sat} \nabla T_\ell \tag{9}$$

where D_ℓ is the diffusivity of salt in water, σ is the Soret coefficient which is taken to be negative when solute moves towards the cold end (this is the case for NaCl and KCl), and C_s^h and C_s^c are the actual concentrations of salt in the liquid adjacent to these two faces (Fig. 7).

The salt flux at the solid-liquid interfaces can be expressed in the general forms:

$$j_s = k_{dis}\, f(\zeta_h) \tag{10a}$$

at the hot (dissolving) face, and

$$j_s = k_{crys} f'(\zeta_c) \tag{10b}$$

at the cold (crystallizing) face.

In these equations, k_{dis} and k_{crys} are phenomonological rate coefficients which describe the interfacial kinetics of dissolution and crystallization. The quantity ζ_h is the fractional undersaturation of the solution at the hot face:

$$\zeta_h = \frac{\left(C_s^{sat}\right)_h - C_s^h}{\left(C_s^{sat}\right)_h} \tag{11a}$$

and ζ_c is the fractional supersaturation at the cold face:

$$\zeta_c = \frac{C_s^c - \left(C_s^{sat}\right)_c}{\left(C_s^{sat}\right)_c} \tag{11b}$$

The various models of interfacial kinetic-limited inclusion migration depend essentially on the types of functions $f(\zeta_h)$ and $f'(\zeta_c)$ chosen to describe dissolution and crystallization kinetics. Once these are specified, the migration velocity can be calculated from the preceding formulas.

Geguzin and coworkers(4) utilized the concept of critical under- and supersaturations below which all interface transport

ceases. The functions f and f' are given by:

$$f(\zeta_h) = \begin{cases} \zeta_h - \zeta^*_{dis} & \text{if } \zeta_h > \zeta^*_{dis} \\ 0 & \text{if } \zeta_h < \zeta^*_{dis} \end{cases}$$

$$f'(\zeta_c) = \begin{cases} \zeta_c - \zeta^*_{crys} & \text{if } \zeta_c > \zeta^*_{crys} \\ 0 & \text{if } \zeta_c < \zeta^*_{crys} \end{cases} \qquad (12)$$

where ζ^*_{dis} is the critical undersaturation required to permit dissolution of the salt and at the hot face ζ^*_{crys} is the critical supersaturation needed to nucleate crystallization at the cold face. These two critical departures from equilibrium are presumed to be properties of the solid-liquid system, as are the associated constants k_{dis} and k_{crys}. Using the functions in Eq(12) in the theory gives the migration velocity:

$$v = \frac{1}{\rho_s} \frac{D_\ell C_s^{sat}}{1 + \mathcal{D}} \left[\left(\frac{1}{C_s^{sat}} \frac{dC_s^{sat}}{dT} - \sigma \right) \nabla T_\ell - \frac{\zeta^*_{dis} + \zeta^*_{crys}}{L} \right] \qquad (13)$$

where

$$\mathcal{D} = \frac{D_\ell C_s^{sat}}{L} \left(\frac{1}{k_{dis}} + \frac{1}{k_{crys}} \right) \qquad (14)$$

is a dimensionless quantity reflecting the relative importance of diffusion in the liquid and interfacial kinetics in the overall transport rate. The theoretical model proposed by Anthony and Cline(3,10) is identical to Geguzin's formulation if the "kinetic potential" utilized by the former authors, K, is a linear function

of inclusion speed (as they suggested):

$$K = K_o + \alpha v \tag{15}$$

The coefficients K_o and α can be identified with the parameters of the Geguzin model in the following manner:

$$K_o = RT(\zeta^*_{dis} + \zeta^*_{crys}) \tag{16}$$

and

$$\alpha = RT\ \rho_s \left(\frac{1}{k_{dis}} + \frac{1}{k_{crys}} \right) \tag{17}$$

Use of these formulas converts the velocity equation derived by Anthony and Cline[Eq(10) of ref. 3] to Eq(13). The parameters K_o and α are equivalent to the critical fractional departures from saturation and the interface transfer coefficients of the Geguzin model. The latter, being amenable to physical interpretation, are preferable.

Figures 8 and 9 show the migration velocities measured in NaCl for a variety of inclusion sizes, temperatures, and temperature gradients. The crystals were unstressed in these experiments.

The last row of Table 1 shows the interfacial kinetic coefficients $(1/k_{dis} + 1/k_{crys})^{-1}$ taken from the results of Refs. 3 and 4 for KCl at 40°C and from the experiments in the present study for NaCl at the same temperature. In all cases, the interfacial kinetic coefficient was deduced from the measured speeds and Eqs.(13) and (14). The physical properties of the NaCl/H_2O system at 40°C needed for the calculation were taken from the literature compilation in Ref. 14. Of these property data, the

Soret coefficient σ is very poorly known and the figure used is only an estimate. However, when used in Eq(13), the Soret effect is found to be 5 times as large as the temperature-dependent solubility term to which it is added. The smallest value of the interfacial kinetic coefficient for NaCl listed in Table 1 corresponds to that determined with a Soret coefficient of $-0.002\ K^{-1}$. If σ is set equal to zero, the largest value in the table is obtained. Given this uncertainty in the Soret effect for NaCl, the best that can be said about the interfacial kinetic coefficient is that it is probably less than that in KCl. A very rough estimate the interfacial kinetic coefficient obtained from the data on Figs. 8 and 9 and Eqs.(13) and (14), yields:

$$\left(\frac{1}{k_{dis}} + \frac{1}{k_{crys}}\right)^{-1} \simeq 3\ e^{-4400/T} \qquad (18)$$

A similar uncertainty does not apply to KCl because the temperature dependence of its solubility in water is ten times larger than that of NaCl so that application of Eq.(13) is not highly sensitive to the Soret coefficient.

The existence of a minimum inclusion size for motion is evident from the data, particularly those shown in Fig. 9. In the Geguzin model, an inclusion cannot move unless the difference in the solubilities between the hot and cold faces exceeds the sum of the critical undersaturation for dissolution and the critical supersaturation for crystallization, or:

$$(C_s^{sat})_h - (C_s^{sat})_c \geq \Delta C^*_{dis} + \Delta C^*_{crys} = C_s^{sat}(\zeta^*_{dis} + \zeta^*_{crys})$$

The left hand side of this formula is given by Eq(7) with $\nabla T_\ell = \frac{3}{2} \nabla T_\infty$ (for an initially cubical inclusion), so the minimum size for motion is:

$$(L_o)_{min} = \frac{2}{3} \frac{\zeta^*_{dis} + \zeta^*_{crys}}{\nabla T_\infty \left(\frac{1}{C_s^{sat}} \frac{dC_s^{sat}}{dT} \right)} \qquad (19)$$

Using the critical fractional departure from saturation given by Table 1, Eq(19) indicates that an initially cubical inclusion in a temperature gradient of $30^oC/cm$ at 40^oC must have a minimum dimension of 22 μm to begin moving. When this inclusion has achieved its terminal velocity and shape, its width is ∿25 μm. The lower set of data in Fig. 9 suggest a critical size for these conditions of about twice this value, or ∿50 μm. As the temperature and temperature gradient increase, the two terms in the denominator of Eq(19) increase and the minimum size for motion decreases. This effect is clearly seen in the data shown in Fig. 9.

NONLINEAR INTERFACE KINETICS

The theory described above assumes that the salt flux at the solid-liquid interface is a linear function of the super- or under-saturation. For small departures from equilibrium, this is probably not true. The power law:

$$f'(\zeta_c) = \zeta_c^r \qquad (20a)$$

is frequently used to represent crystallization kinetics at the surface of positive crystals. This formulation encompasses the theory of Burton, Cabrerra and Frank(11), according to which r approaches 2 at low supersaturation and tends towards unity at high

supersaturation. Equation (20a) is also a good approximation to the birth-and-spread model of crystallization over a limited range of supersaturation(12). We assume that a formulation similar to Eq(20a) applies for the dissolution process, or:

$$f(\zeta_h) = \zeta_h^r \tag{20b}$$

Because an inclusion is equivalent to a negative crystal, growth steps are readily available at the edges of the side facets adjacent to the cold face, so that crystallization should be relatively easy. However, steps for dissolution are difficult to form on the hot face(13). Therefore, it is expected that $k_{crys} >> k_{dis}$, or the rate-limiting surface kinetic step is that associated with dissolving the crystal at the hot side of the inclusion.

Equation(20) can be used in the migration velocity analysis with the additional specification r = 2 to conform with the low-ζ limit of the BCF theory. The velocity is found to be:

$$v = \frac{D_\ell C_s^{sat}}{4L\rho_s} \mathcal{D} \left\{ \sqrt{1 + \frac{4L\nabla T_\ell}{\mathcal{D}} \left(\frac{1}{C_s^{sat}} \frac{dC_s^{sat}}{dT} - \sigma \right)} - 1 \right\}^2 \tag{21}$$

where the parameter characterizing the relative magnitudes of the resistances due to liquid diffusion and interfacial kinetics is:

$$\mathcal{D} = \frac{D_\ell C_s^{sat}}{L} \left(\frac{1}{\sqrt{k_{crys}}} + \frac{1}{\sqrt{k_{dis}}} \right)^2 \tag{22}$$

The limit of surface kinetic control is obtained by setting $\mathcal{D}>>1$ in Eq.(21):

$$v = \frac{1}{\rho_s}\left(\frac{1}{\sqrt{k}_{crys}} + \frac{1}{\sqrt{k}_{dis}}\right)^{-2}\left(\frac{1}{C_s^{sat}}\frac{dC_s^{sat}}{dT} - \sigma\right)^2 \left(L\nabla T_\ell\right)^2 \qquad (23)$$

For liquid diffusion control ($\mathcal{D}<<1$), Eq.(21) reduces to:

$$v = \frac{D_\ell C_s^{sat}}{\rho_s}\left(\frac{1}{C_s^{sat}}\frac{dC_s^{sat}}{dT} - \sigma\right)\left(\nabla T_\ell\right) \qquad (24)$$

DISCUSSION

Figure 10 compares earlier data on brine inclusion migration in single crystal KCl and the measurements in NaCl crystals obtained in the present study. The ordinate on this graph is the velocity per unit temperature gradient at the center of the inclusion (i.e., ∇T_ℓ), which was obtained from the applied temperature gradient and the inclusion dimensions by use of Fig. 4. Deferring until later discussion of the three curves on this plot, the most striking feature of the data is their very large scatter - the typical spread in migration velocities for nominally identical experimental conditions is nearly an order of magnitude. Part of the scatter is due to the large variability in the velocity of small inclusions which are close to the critical size where motion in a specified ∇T_∞ is impossible(Fig. 9). However, even for large inclusions which move readily in the applied temperature gradient, substantial variability in velocity is observed.

This scatter is believed to be inherent in the phenomenon and to

be due to the stochastic nature of the dissolution process. According to the BCF theory, the rate of removal of solid from the hot face of the inclusion depends upon the presence of dislocations intersecting this surface. Dissolution steps are provided by both screw and edge dislocations. Assuming a dislocation density of 10^5 cm^{-2} and an inclusion 50 μm wide, the average number of dislocations intersecting the dissolving face of a typical inclusion examined here is 2.5. Therefore, substantial differences in the coefficient k_{dis} can be expected from one inclusion to another due solely to the statistical variations of this number. In the growth of small crystals this phenomenon has been observed and is termed "growth dispersion" (12).

In addition, the dissolution rate will in general be different for two inclusions which are intersected by the same number of dislocations on the hot face; the temperature gradient, and hence the temperature, vary considerably over the face perpendicular to the thermal gradient. Hence, a dislocation near the axis will be a more prolific source of dissolution steps than one near the edge of the inclusion. Thus, the number and the location of the dislocations intersecting the hot face of the inclusions are believed to be responsible for the average velocity under specified conditions as well as the dispersion about this average value. The additional experimental results described below support this general interpretation of inclusion migration.

Figure 11 shows the migration velocity of a single inclusion in KCl which was followed for 72 hours. Periodic measurement of the

position of the inclusion allowed the average speed between successive observations to be determined. These average velocities are shown as the horizontal line segments on Fig. 11. The long segments indicate a large interval between measurements; they do not imply that the inclusion velocity was constant over this interval. The velocity of the inclusion followed in this test changed by a factor of four, from a minimum value of $\sim$ 8 μm/hr to a maximum of $\sim$ 32 μm/hr. The change was fairly smooth - the velocity tended to increase or decrease continuously for long periods of time. This behavior is most easily interpreted in terms of the dynamic interaction between the inclusion and dislocations in the crystal.

The pattern shown on Fig. 11 can be rationalized in the manner shown schematically in Fig. 12. At time zero, we imagine that the hot face of the inclusion is intersected by a single dislocation (No. 1) close to the center of the face. In general, the dislocation does not intersect the surface at 90^{o} so that as the inclusion moves, the intersection point moves further off-axis. At off-axis positions, ∇T_{ℓ} is less than it is close to the axis and hence the inclusion slows down. Somewhere between 8 and 20 hours the inclusion picks up another dislocation, designated as No. 2 in Fig. 12. The three dislocation intersections with the dissolving face result in a several-fold increase in the inclusion velocity. As the intersections of the No. 2 dislocation with the hot face move off-axis, the inclusion again begins to slow down. The inclusion followed in Fig. 11 seems to be capable of sustaining a minimum speed of $\sim$ 8 μm/hr, which may represent the velocity in the absence of any dislocation

intersection with the dissolving hot face. Although the scenario described above is only illustrative, it is clear that the dislocation hypothesis is consistent with the stochastic nature of the measured inclusion velocities.

Figure 13 shows the effect of doubling the unaxial stress on the crystal during the migration process. At the time of the stress increase, the migration velocities of the three inclusions being followed jumped abruptly and continued to increase with time under the higher load. This behavior is attributed to the activation of dislocation sources in the crystal by the increase in load and their continued movement by creep at the high load. As a result of the increased dislocation motion, more dislocation intersections with the inclusions occurred, thereby decreasing the resistance to dissolution of the hot face for the prevailing undersaturation and increasing the inclusion speed. The velocities do not return to their initial values upon removal of the load, so the effect is not elastic.

Tests were made to distinguish between control of the migration velocity by liquid diffusion and by interfacial kinetics. In these tests, several inclusions were selected and the applied temperature gradient ∇T_∞ was varied while keeping the temperature in the vicinity of the inclusions constant. Each time ∇T_∞ was changed, the inclusions changed shape because $L \propto \nabla T_\infty^{-1/2}$ and $W^2 L$ = constant. For each ∇T_∞, the inclusion shape was measured and the centerline ∇T_ℓ was calculated by the method described earlier. Plots of velocity versus ∇T_ℓ were not linear as predicted for diffusion control [(Eq.(24)].

For interface kinetic control, the velocity should depend upon the product $L\nabla T_\ell$ raised to some power other than one. Figure 14 shows the velocities of three inclusions plotted in this manner for tests in which the mean temperature was held constant at 50^o C but the applied temperature gradient varied. The slopes on the log-log plots are 3.0 for two of the inclusions and 1.6 for the third. Fig. 15 gives the results of more extensive testing of another inclusion at a temperature of 63^o C. In this case the slope is 2.2, which is quite close to the exponent of 2 predicted by the BCF model (Eq. 23).

Another demonstration that interface kinetics dominate the salt transport process is the comparison of diffusion-limited theory with the data shown in Fig. 10. Curves 1 and 2 represent $v/\nabla T_\ell$ calculated from Eq. (24) for NaCl and KCl, respectively. These two diffusion-limited theoretical curves are between one and two orders of magnitude larger than the corresponding data representing small inclusions in the alkali halide single crystals. Curve 3 is Jenks' (15) empirical formula for $v/\nabla T_\infty$ based on the data of Bradshaw and Sanchez (16). The agreement between curves 1 and 3 is remarkable, considering that the latter needs to be shifted by a typical thermal gradient amplification factor of 2 - 3 to place both curves on the same basis. Since Jenks' curve is based on Bradshaw and Sanchez' data and the theoretical curve 1 is for purely diffusion-limited migration, it follows that the inclusions observed by Bradshaw and Sanchez were in fact moving at this limiting speed. The inclusions studied by Bradshaw and Sanchez were large (typical dimension of 1 mm) in natural crystals. Even if

Even if this material had a dislocation density as low as that of the synthetic single crystals (10^5 cm^{-2}), the faces of each inclusion would have been intersected by $\sim 10^3$ dislocations. This number is to be compared with the average of 2.5 dislocations intercepted by the dissolving faces of the inclusions in the experiments utilizing synthetic crystals. Diffusion control is expected for the large inclusions, which are intersected by enough dislocations to reduce the kinetic resistance to salt dissolution to negligible values. In general, the rate-limiting process in thermal gradient migration of inclusions in brine depends both on the size of the inclusion and on the dislocation density of the solid in which it moves.

CONCLUSIONS

The migration velocity of liquid inclusions in single crystal NaCl is nearly two orders of magnitude lower than that in KCl at 40°C. This difference is due in approximately equal measure to the lower temperature coefficient of salt solubility in water and to the lower interfacial kinetic coefficient in NaCl than in KCl. The slow interfacial kinetic step, which is probably associated with dissolution at the hot face of the inclusion, accounts for over 90% of the total resistance to salt transport in NaCl.

The migration velocity varies approximately as the square of the temperature gradient rather than linearly as suggested by the theory of Anthony and Cline and Geguzin et al. The nonlinear dependence is in accord with the Burton-Cabrerra-Frank model of crystallization catalyzed by dislocations emerging at the interface. Because of the small sizes of the inclusions produced in synthetic single crystals and the low dislocation density of this material, the

dissolving faces of the inclusions are intersected by less than three dislocations. Random variations in this number account for significant variations in the velocity of a single inclusion with time and for the scatter in the velocities measured for a number of different inclusions subjected to the same conditions.

Neither the linear interface kinetic theory of Anthony and Cline and Geguzin et al, nor the nonlinear BCF theory can completely account for the observations. The critical departure from saturation in the former theory is necessary to explain the inability of a platelet-shaped inclusion to recover a perfectly cubical shape after removal of the temperature gradient and the immobility of small inclusions in a temperature gradient. On the other hand, the variation of the inclusion speed with the temperature gradient, the large variability of inclusion speeds measured under identical macroscopic conditions, and the effect of mechanical loading of the crystal on the speed are best rationalized by the BCF model.

ACKNOWLEDGEMENT

This work was supported by the U.S. Department of Energy through the Office of Basic Energy Sciences and the Office of Nuclear Waste Isolation, under Contract W-7405-ENG-48.

APPENDIX-INCLUSION SHAPES

An inclusion in a temperature gradient takes the shape of a square disk of thickness L along the gradient and width W in the transverse direction. Figure A-1 shows a perturbation of this shape caused by transfer of dn moles of salt from the lateral faces (point 1) to the rear face (point 2). The change in the

dimension W is obtained from:

$$dn = 4\ \rho_s\left(\frac{dW}{2}\ WL\right) = 2\ \rho_s WL dW \qquad \text{(A-1)}$$

and since the volume LW^2 of the inclusion is constant,

$$dL = -\ \frac{2L}{W}\ dW \qquad \text{(A-2)}$$

The stability condition is obtained by equating the free energy change (or reversible work) due to transfer of salt from concentration C_1 at point 1 to C_2 at point 2 to the work required to distort the W and L dimensions of the inclusion by dW and dL, respectively. The latter is due to an increase in surface area.

Work done by Transferring Salt from C_1 to C_2

The change in chemical potential as salt is transferred from C_1 to C_2 is equal to the reversible work made available. The salt concentration in the liquid at the corner between the hot face and the sides is:

$$C_1 = \left(C_s^{sat}\right)_1 - \Delta C^*_{dis} \qquad \text{(A-3)}$$

Since the system is stationary and the flux between the side and rear faces is zero, the difference between the brine concentration and the saturation concentration at point 1 $\left[\left(C_s^{sat}\right)_1\right]$ is just equal to the critical undersaturation for dissolution, ΔC^*_{dis}. Similarly at the depositing face, the liquid concentration is:

$$C_2 = \left(C_s^{sat}\right)_2 + \Delta C^*_{crys} \qquad \text{(A-4)}$$

where $\left(C_s^{sat}\right)_2$ is the salt solubility at the temperature of the rear face and ΔC^*_{crys} is the critical supersaturation for crystallization.

The change in salt chemical potential per mole transferred from the lateral face to the rear face is $RT\ln(C_2/C_1)$. When multiplied by the number of moles transferred(Eq.(A-1)), the work available is:

$$dW_\ell = -RT\ln(C_2/C_1)dn \tag{A-5}$$

The difference in the saturated salt concentrations at points 1 and 2 is assumed to be due to a temperature difference $\nabla T_\infty L$; because the transfer is assumed to occur near the edges of the inclusion, the temperature gradient is closer to ∇T_∞ of the solid than it is to ∇T_ℓ at the center of the platelet. Similarly, the distance between points 1 and 2 is assumed to be approximately equal to the inclusion thickness L. These simplifications yield:

$$\left(C_s^{sat}\right)_1 - \left(C_s^{sat}\right)_2 \simeq \frac{dC_s^{sat}}{dT} \nabla T_\infty L \tag{A-6}$$

Substituting Eqs(A-3) and (A-4) into Eq.(A-5) and using the above approximation result in:

$$dW_\ell = (2WLdW)\ \rho_s RT\left[\frac{1}{C_s^{Sat}} \frac{dC_s^{sat}}{dT} \nabla T_\infty L - \left(\zeta^*_{dis} + \zeta^*_{crys}\right)\right] \tag{A-7}$$

where $\zeta^*_{dis} = \Delta C^*_{dis}/C_s^{sat}$ is the fractional critical undersaturation for dissolution and $\zeta^*_{crys} = \Delta C^*_{crys}/C_s^{sat}$ is the fractional critical supersaturation for crystallization.

Surface Work to Change the Aspect Ratio

The surface energy of the system is:

$$W_s = \gamma A \tag{A-8}$$

where γ is the specific surface energy of the (100) faces which form the sides of the inclusion and A is the surface area:

$$A = 4WL + 2W^2 \tag{A-9}$$

The work to distort the inclusion from (L,W) to (L+dL,W+dW) is:

$$dW_s = \gamma dA = \gamma(4WdL + 4LdW + 4WdW)$$

With dL given by Eq(A-2), this becomes:

$$dW_s = 4\gamma(W - L)dW \tag{A-10}$$

Equilibrium Shape in a Temperature Gradient

The criterion of the equilibrium shape is

$$dW_\ell = dW_s \tag{A-11}$$

or, using Eqs(A-7) and (A-10),

$$\frac{1}{C_s^{sat}} \frac{dC_s^{sat}}{dT} \nabla T_\infty L = \frac{2\gamma}{\rho_s RT} \frac{W - L}{WL} + \left(\zeta^*_{dis} + \zeta^*_{crys}\right) \tag{A-12}$$

Neglecting the last term in Eq(A-12) and assuming W>>L, this formula reduces to Eq(5) of the text.

Shape Relaxation on Removal of the Temperature Gradient

When the temperature gradient is removed, the inclusion tends to relax towards a cubical shape. However, a perfect cube is never attained because the critical concentration differences for dissolution and crystallization provide a free energy barrier which cannot be overcome by the surface work available from relaxation of a slightly noncubical parallelepiped to a perfect cube. The relaxation process is essentially the reverse of the one depicted in Fig. A-1 for establishment of the inclusion shape in a temperature

gradient. An analysis similar to that given above leads to an equation for a terminal relaxed shape given by Eq(A-12) with $\nabla T_\infty = 0$. In addition, since the fluxes in approaching this state are the reverse of those in deforming the inclusion in a temperature gradient, the sign of the last term on Eq(A-12) is negative. The departure from cubical shape is given by Eq(6) of the text.

References

1. J. J. Hohlfelder and G. R. Hadley, "Laboratory Studies of Water Transport in Rock Salt", SAND79-2434 (1979)

2. E. Roedder and H. E. Belkin, "Migration of Fluid Inclusions in Polycrystalline Salt under Thermal Gradients", in Proc. of the 1980 NWTS Progr. Info. Mtg., ONWI-212, p 361 (1980)

3. T. R. Anthony and H. E. Cline, J. Appl. Phys. 42, 3380 (1971)

4. Ya.E. Geguzin, A. S. Dzyuba, and V. S. Korzhanov, Sov. Phys. Crystallogr, 20, 234 (1975)

5. Johnston, W. F., "Dislocation Etch Pits in Non-Metallic Crystals" in Prog. Cer. Sci. 2, J. E. Burke Editor, Pergamon Press (1961)

6. Mendelson, S., J. Appl. Phy. 32, 1579 (1961)

7. Moran, P. R., J. Appl. Phy. 29, 1768 (1958)

8. E. C. Stoner, Phil. Mag., Ser. 7, 36, 803 (1945)

9. H. E. Cline and T. R. Anthony, Acta Metallurgica 19, 175 (1971)

10. H. E. Cline and T. R. Anthony, J. Appl. Phys., 43, 10 (1972)

11. P. Bennema and G. H. Gilmer in "Crystal Growth: an Introduction", P. Hartman, Ed., North-Holland (1973)

12. J. Garside, in "Kinetics of Crystallization From Solution", Current Topics in Materials Science, Editor, E. Kaldis, v. 2, (1977)

13. W. R. Wilcox in "Preparation and Properties of Solid State Materials", Vol. 1, R. A. Lefever, Ed., (1971)

14. D. R. Olander, A. J. Machiels and S. Yagnik, "Thermal Gradient Brine Inclusion Migration in Salt", Final Report, ONWI- (1980)

15. G. H. Jenks, "Effects of Temperature Gradient, Stress, and Irradiation on Migration of Brine Inclusions in a Salt Repository", ORNL -5526 (1979)

16. R. L. Bradshaw and F. Sanchez, "Brine Migration Studies", p. 32, ORNL-4316 (1968)

FIGURE CAPTIONS

1. Microscope and Hot Stage Attachment for Measurement of Inclusion Motion in Alkali Halide Single Crystals

2. Dislocation Etch Pits on the NaCl (100) Surface

3. Platelet-shaped All-Liquid Inclusions in a KCl Crystal

4. Temperature Gradient Amplication Factor. $k_s/k_\ell = 6.4$

5. Change in Inclusion Shape when Subjected to a Temperature Gradient

6. Variation of the Terminal Inclusion Thickness with Temperature Gradient

7. Section of a Liquid-filled Inclusion in a Solid Supporting a Temperature Gradient

8. Velocities of Inclusions in NaCl at a Fixed Temperature Gradient; no Axial Load

9. Velocities of Inclusions in NaCl for Various Temperatures and Temperature Gradients; no Applied Load

10. Migration Speeds per Unit Temperature Gradient (∇T_ℓ) of All-Liquid Inclusions. Curves 1 and 2 are Diffusion-Limited Theoretical Predictions for NaCl and KCl, Respectively. Curve 3 is the Empirical Formula Proposed by Jenks(15) for Large Inclusions in Natural Salt (based on ∇T_∞).

11. Variation of the Migration Velocity of An Inclusion in KCl

12. Schematic Explanation of the Mechanism of the Effect of Dislocation Intersections on the Velocity of Inclusions in Solids

13. Effect of Doubling the Mechanical Load on a Salt Crystal Containing Inclusions Migrating in a Temperature Gradient

14. Effect of Temperature Gradient on the Velocities of Three Inclusions in KCl at 50°C

15. Effect of Temperature Gradient on the Velocity of an Inclusion in KCl at 63°C.

A-1 Perturbation of the equilibrium shape of an inclusion in a temperature gradient.

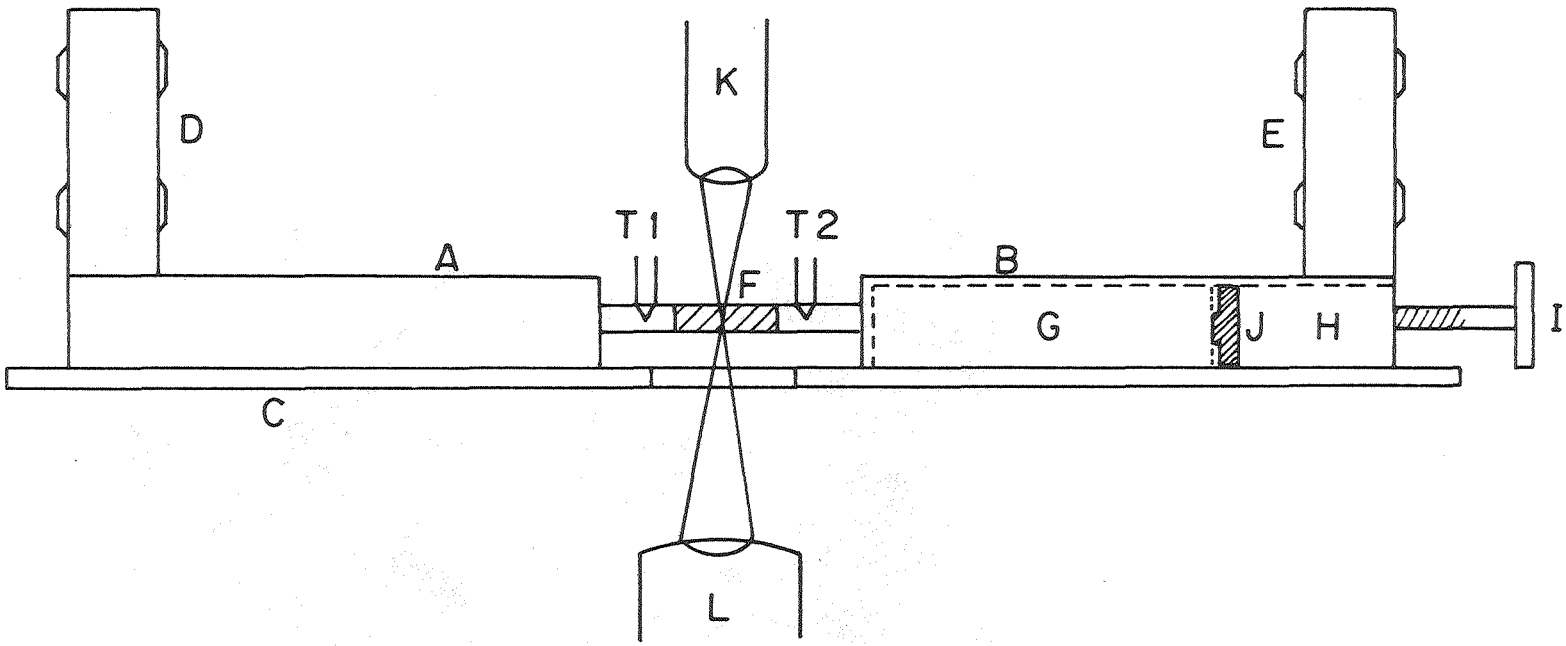

A, B Copper electrodes
C Insulator plate
D, E Clam-shell heaters
F Crystal
G, H Inner copper blocks
I Knob to control load
J Load-cell
K Microscope objective lens
L Microscope condenser
T1, T2 Thermocouples

XBL809-5916

Fig. 1

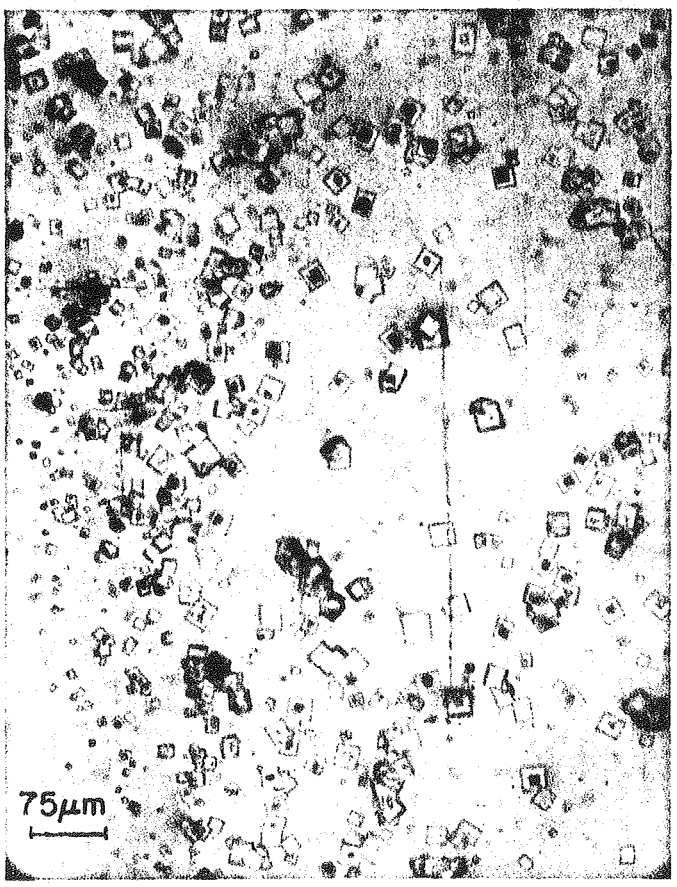

Fig. 3

Fig. 3

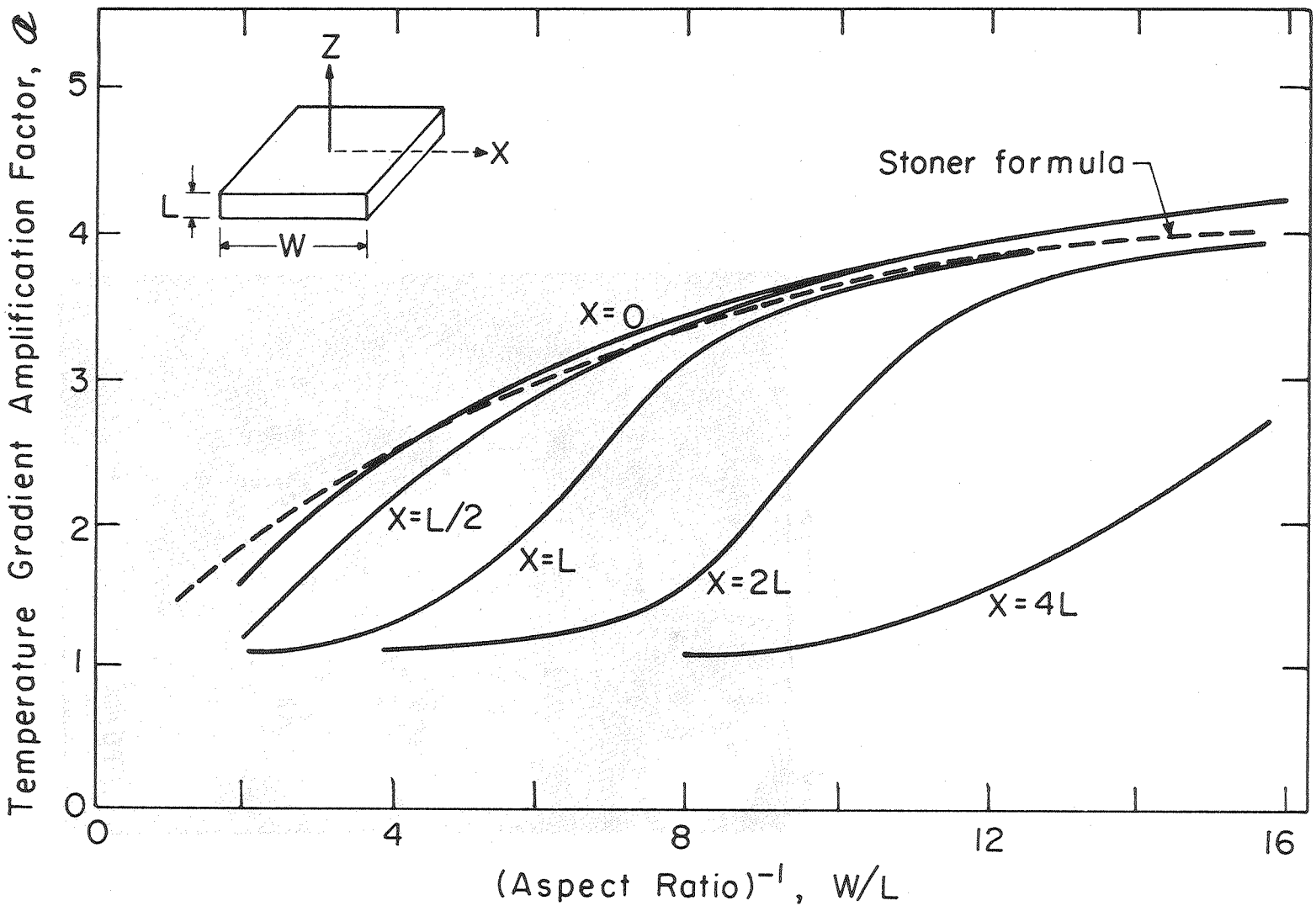

Fig. 4

XBL 8010-6067

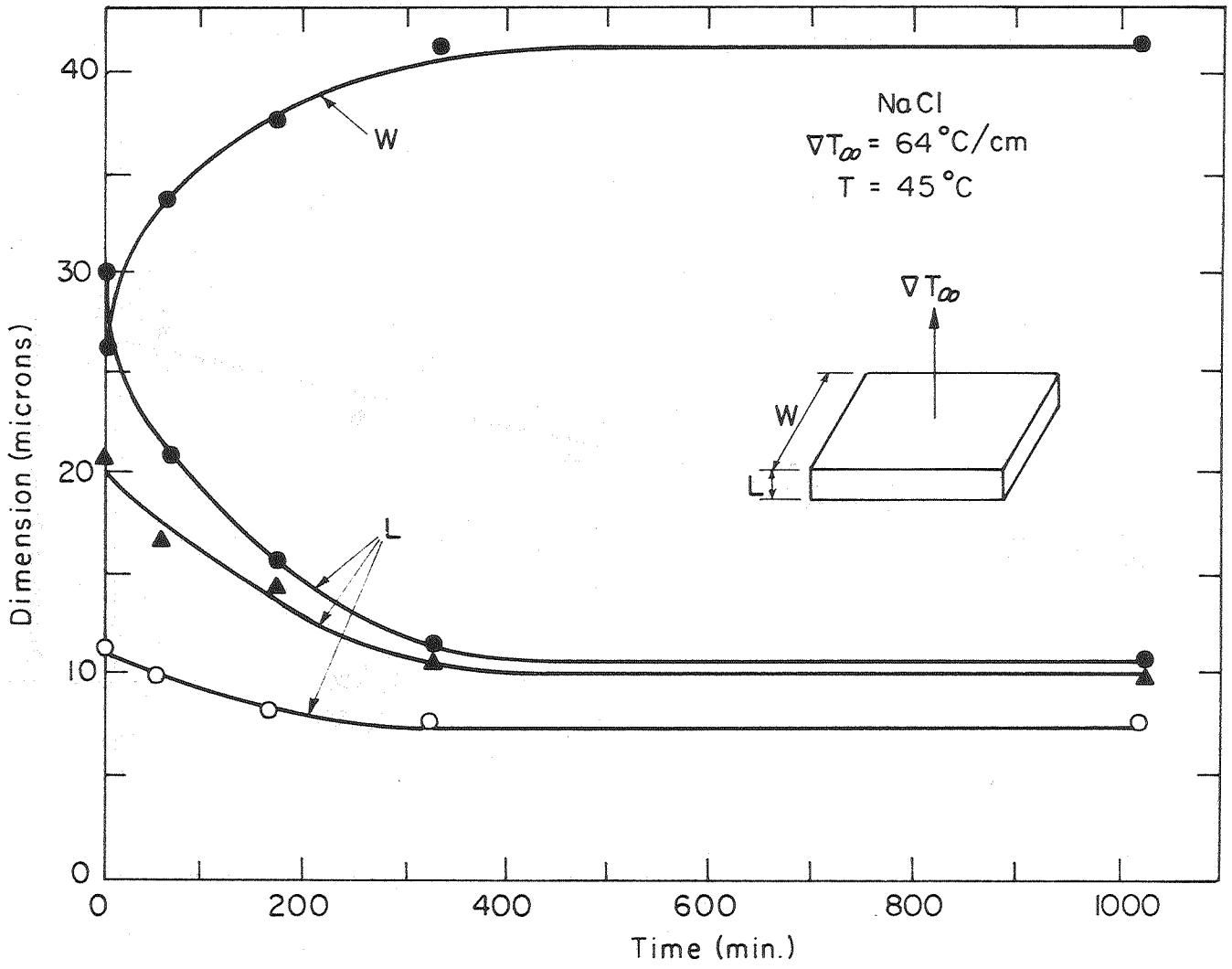

Fig. 5

XBL 796-3568

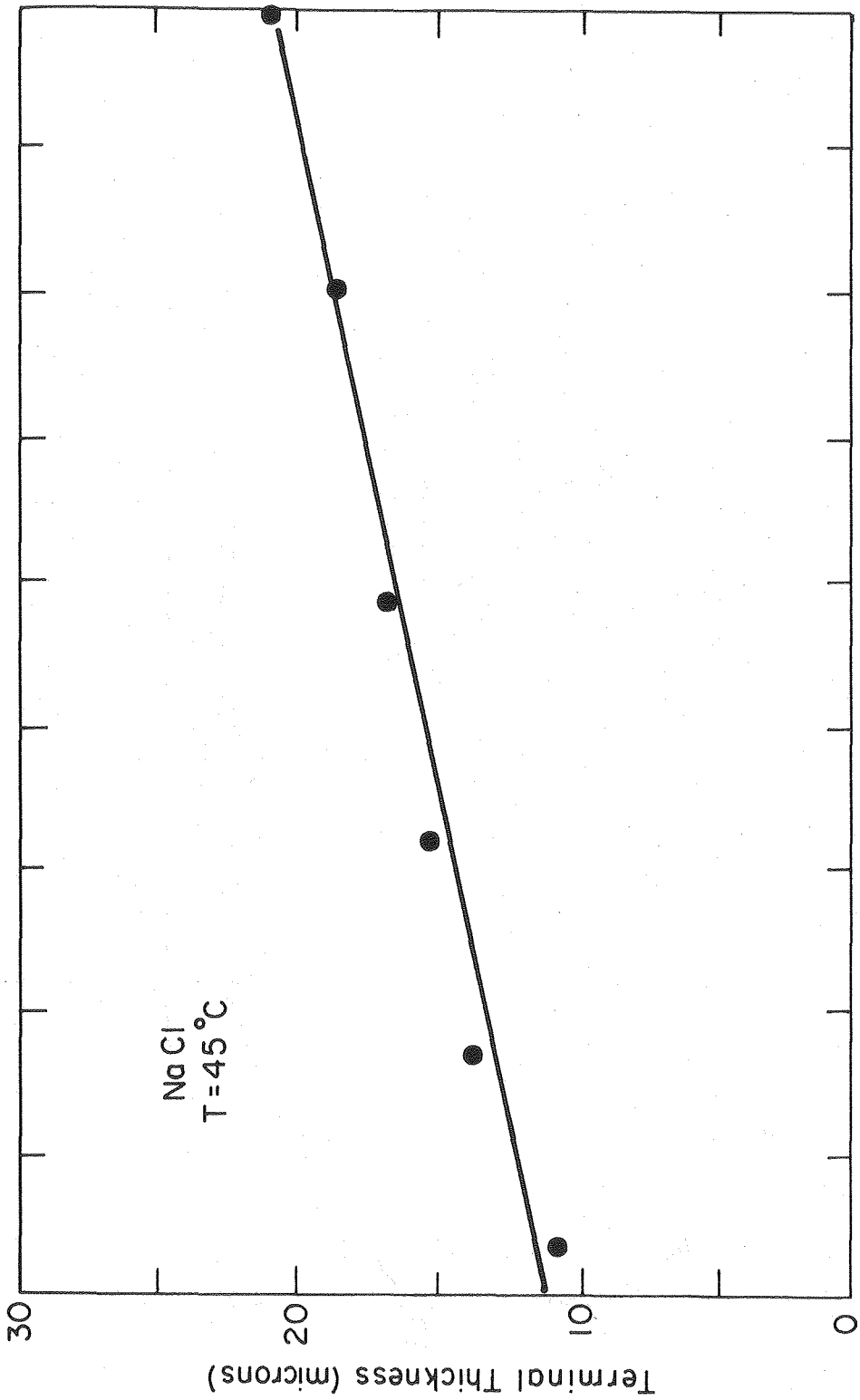

XBL 796-3569

Fig. 6

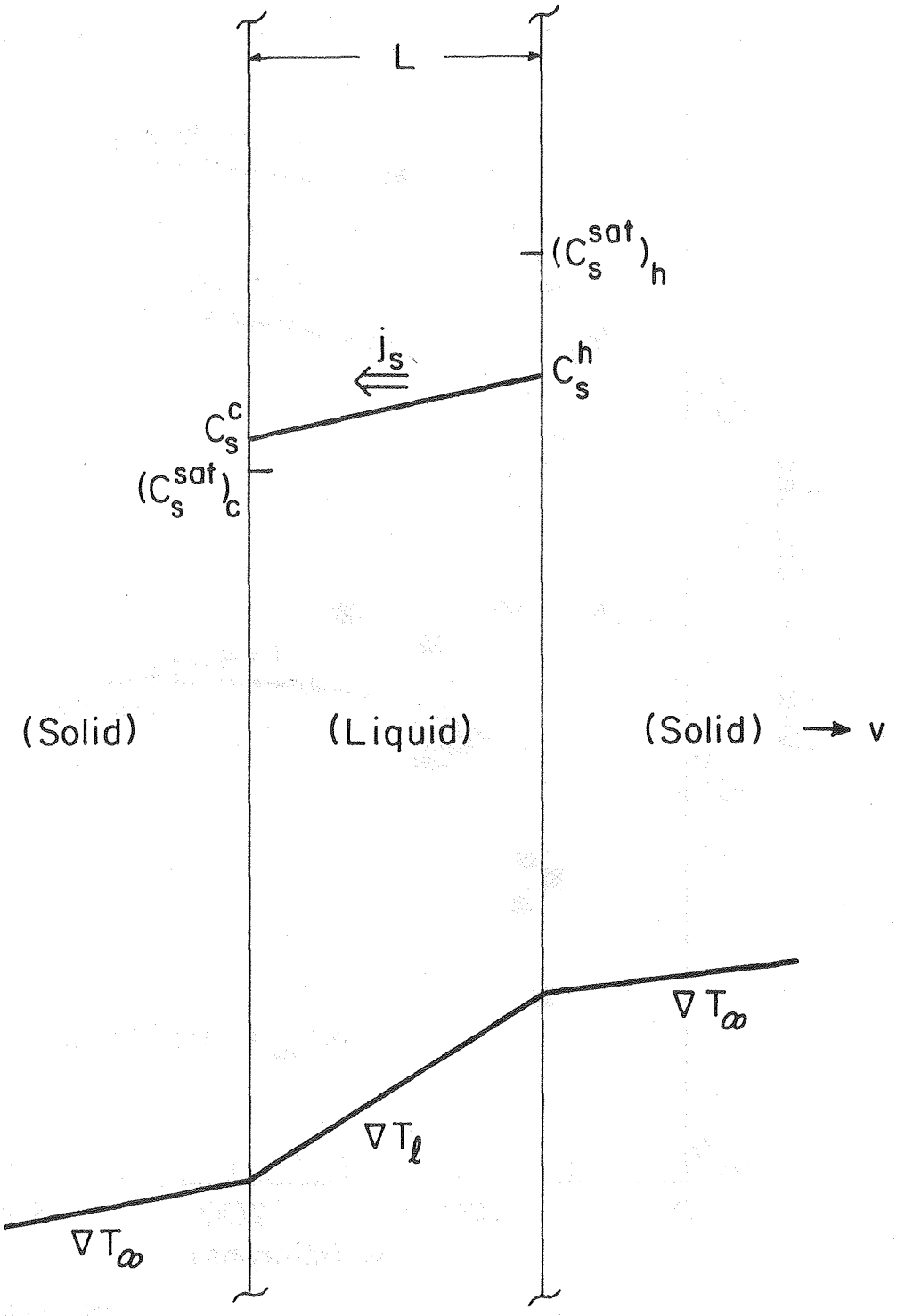

XBL 8010-6066

Fig. 7

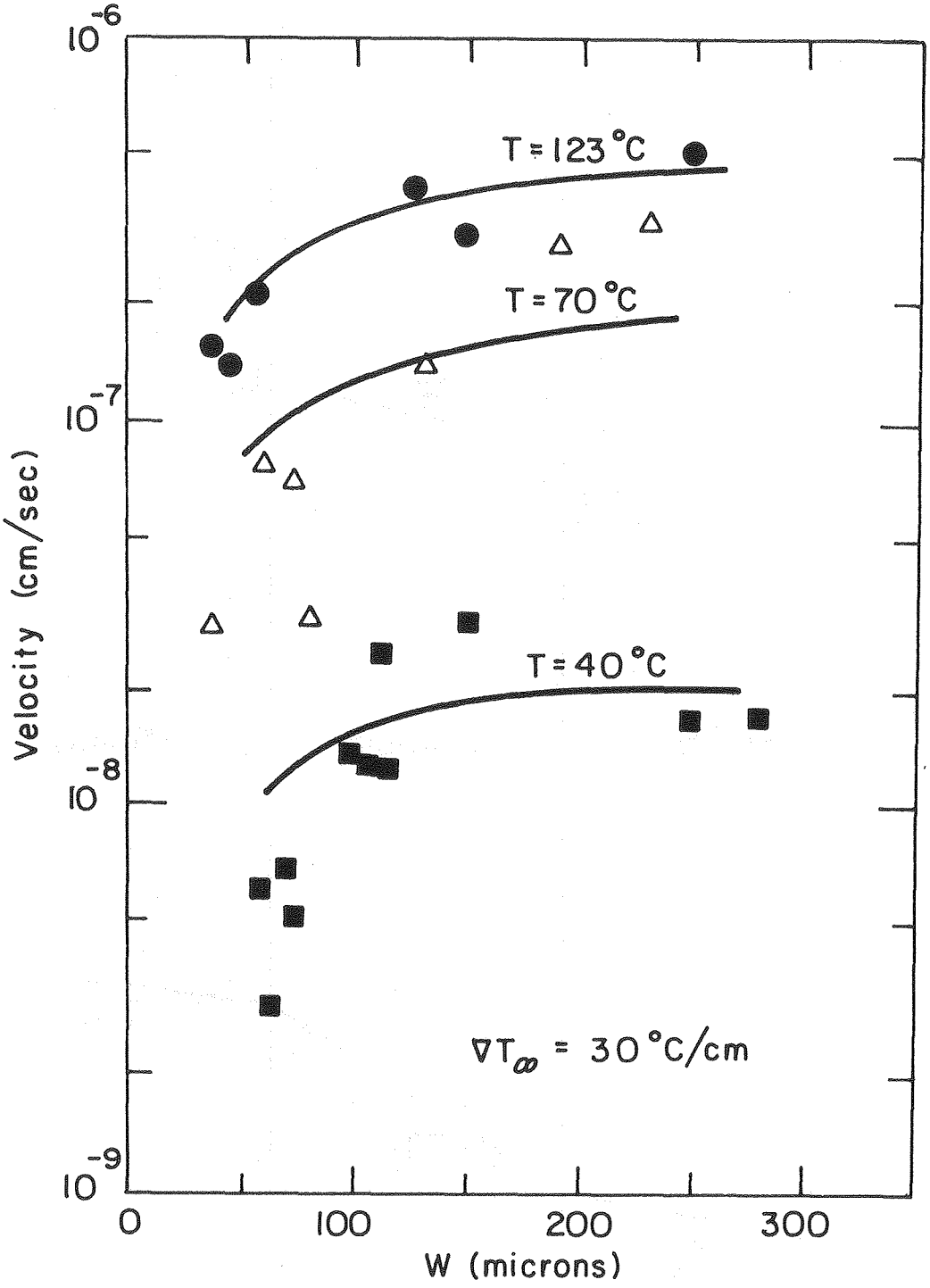

Fig. 8

XBL 796-3574

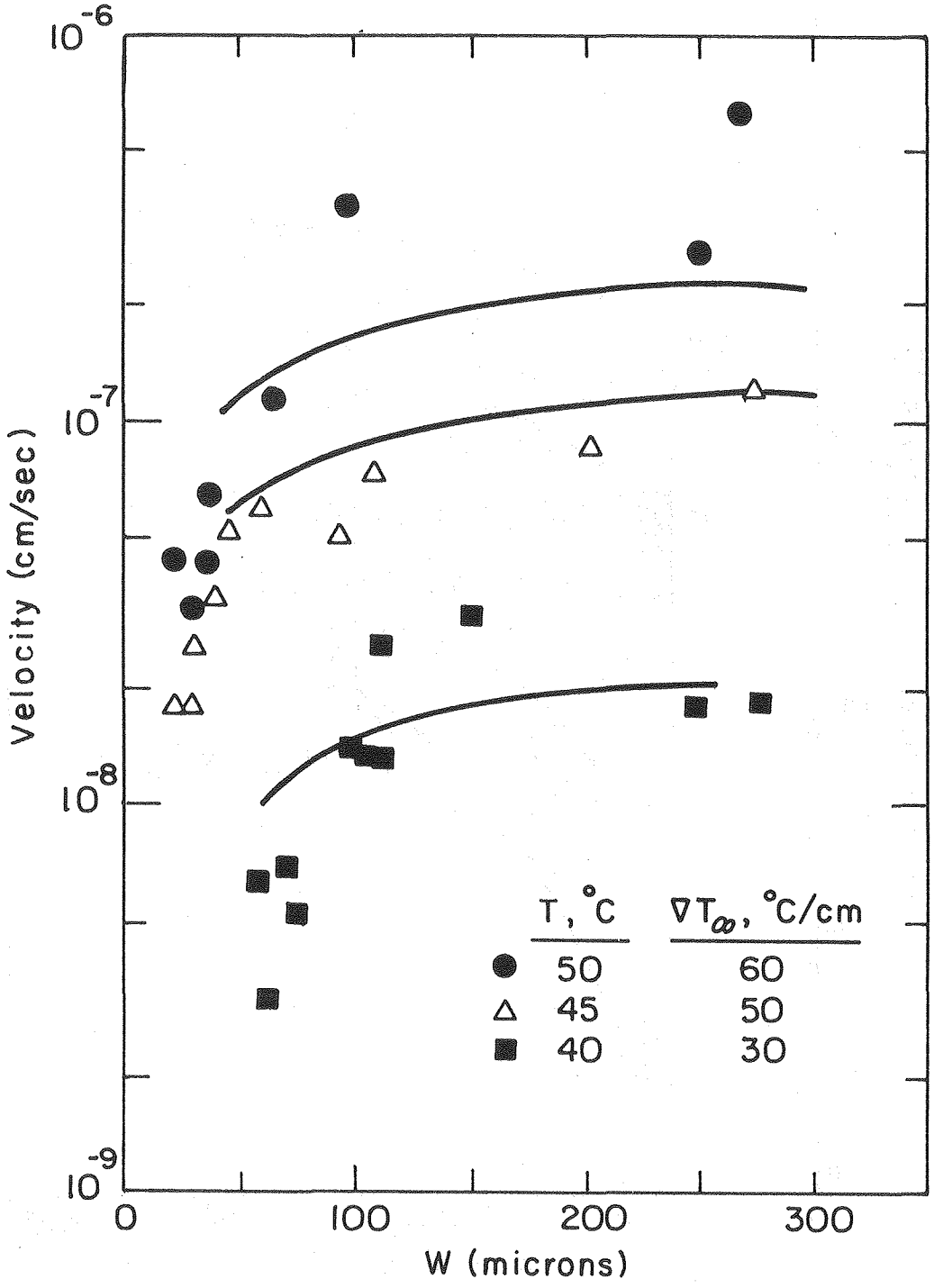

Fig. 9 XBL796-3573

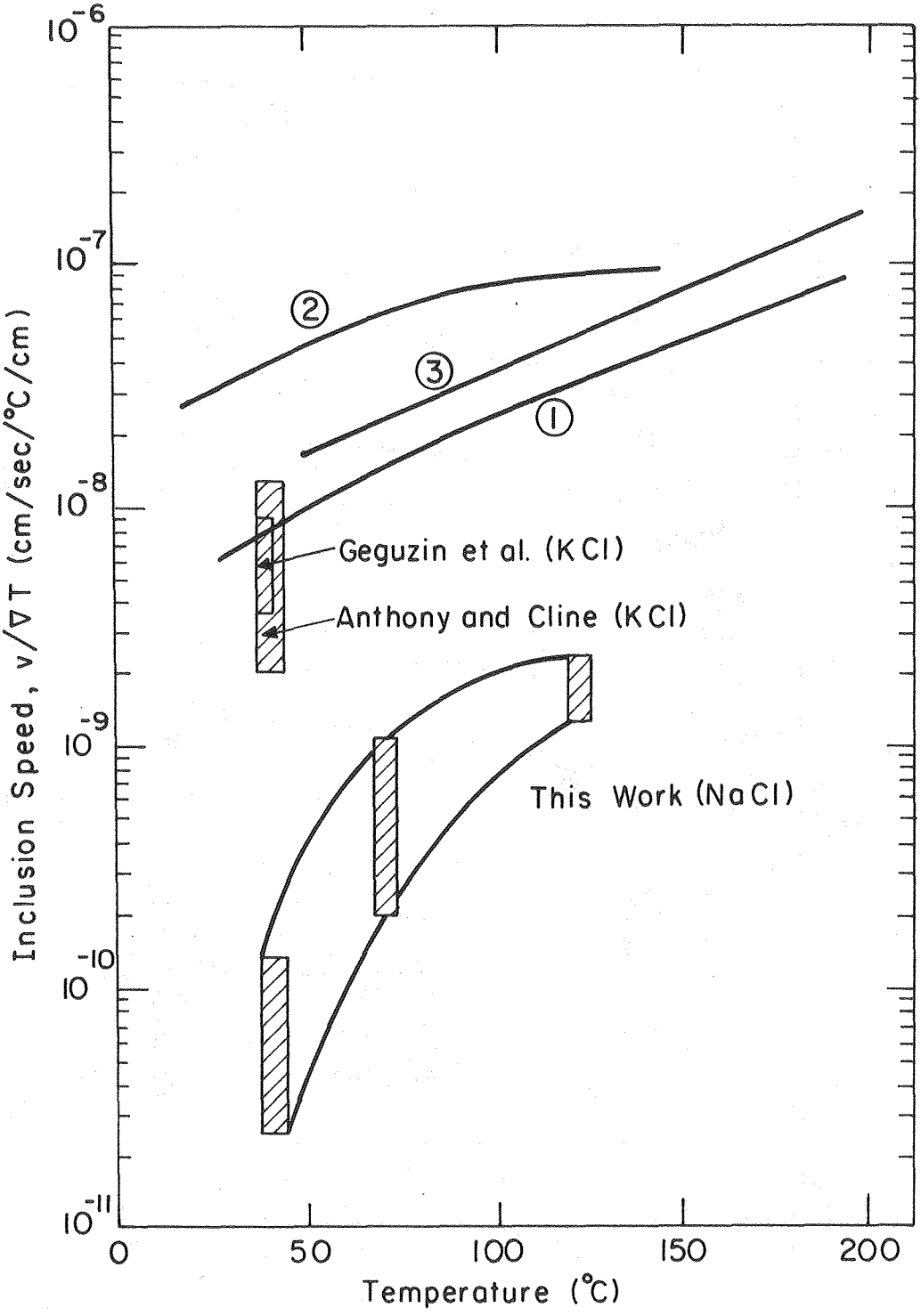

Fig. 10

XBL 8010-6069

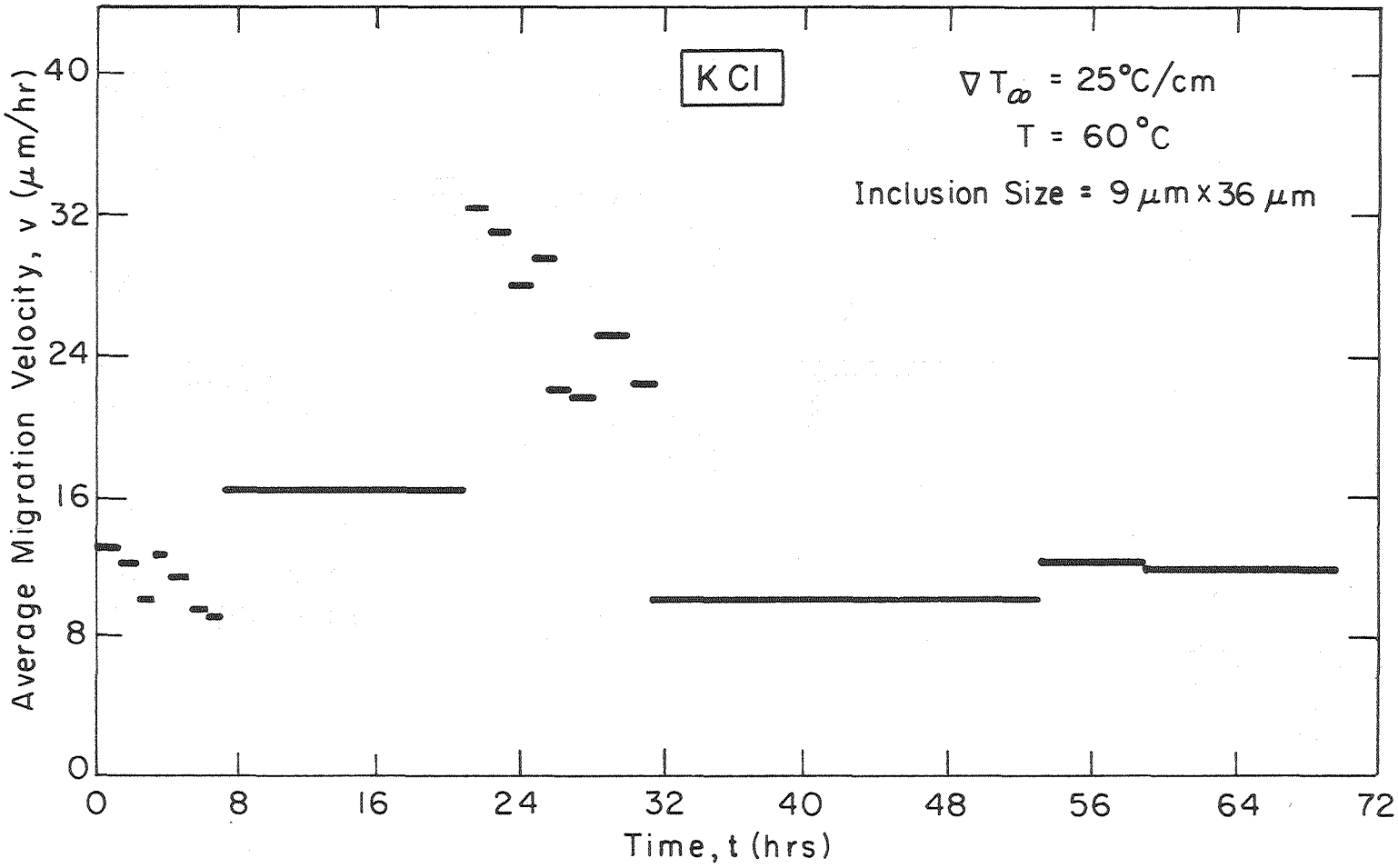

Fig. 11

XBL808-5646

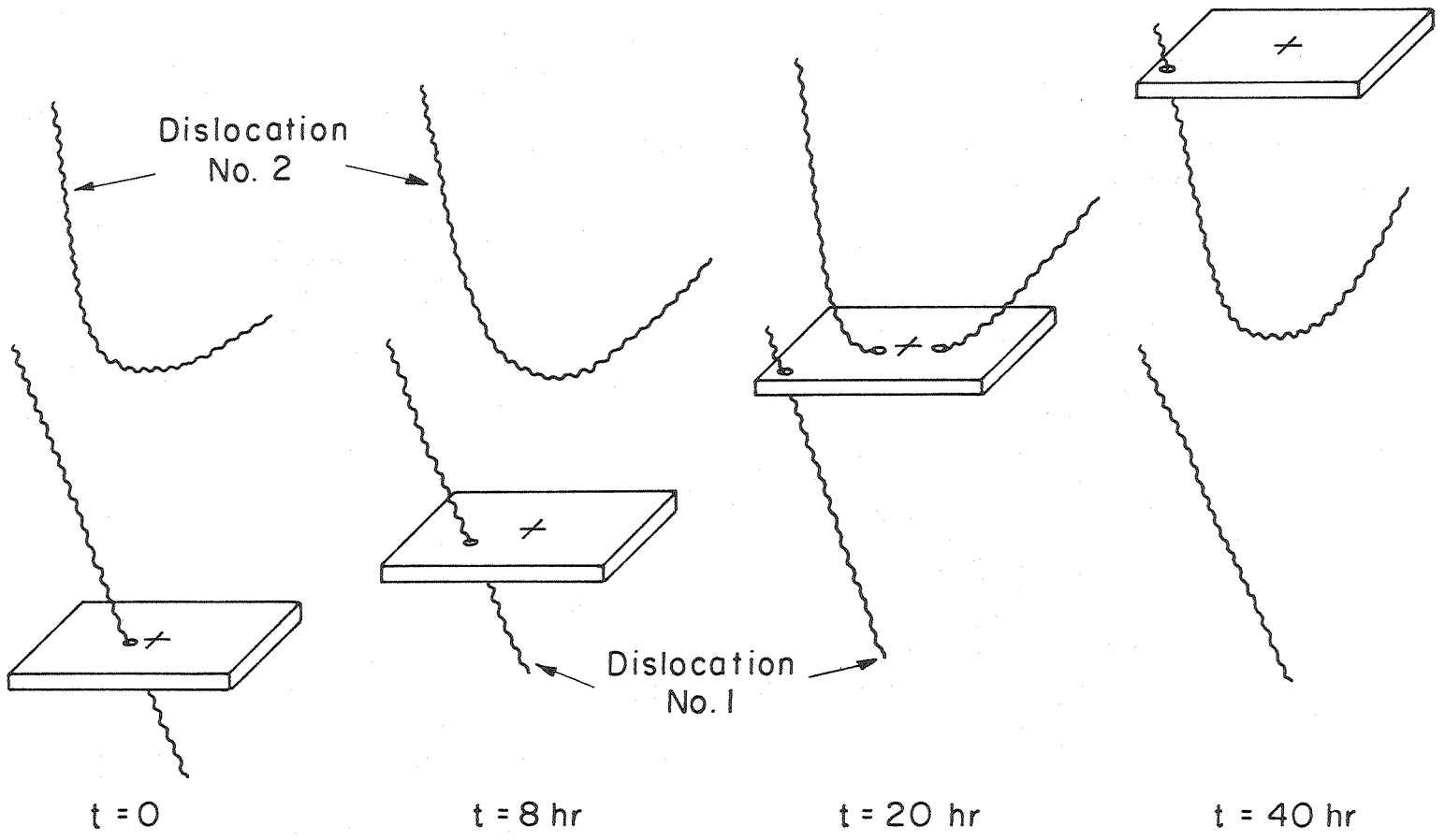

Fig. 12

XBL 8010-6068

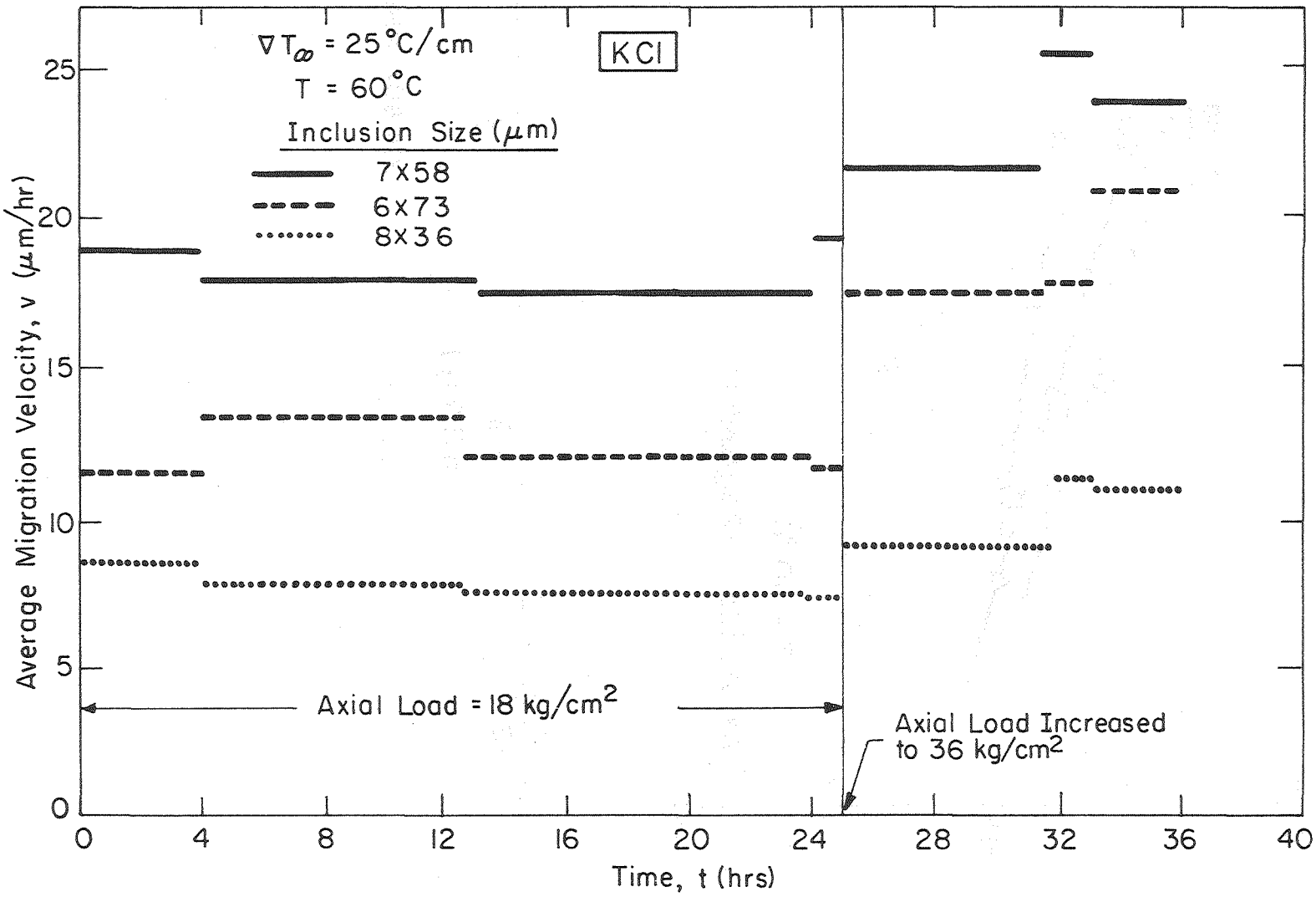

Fig. 13

XBL 808-5645

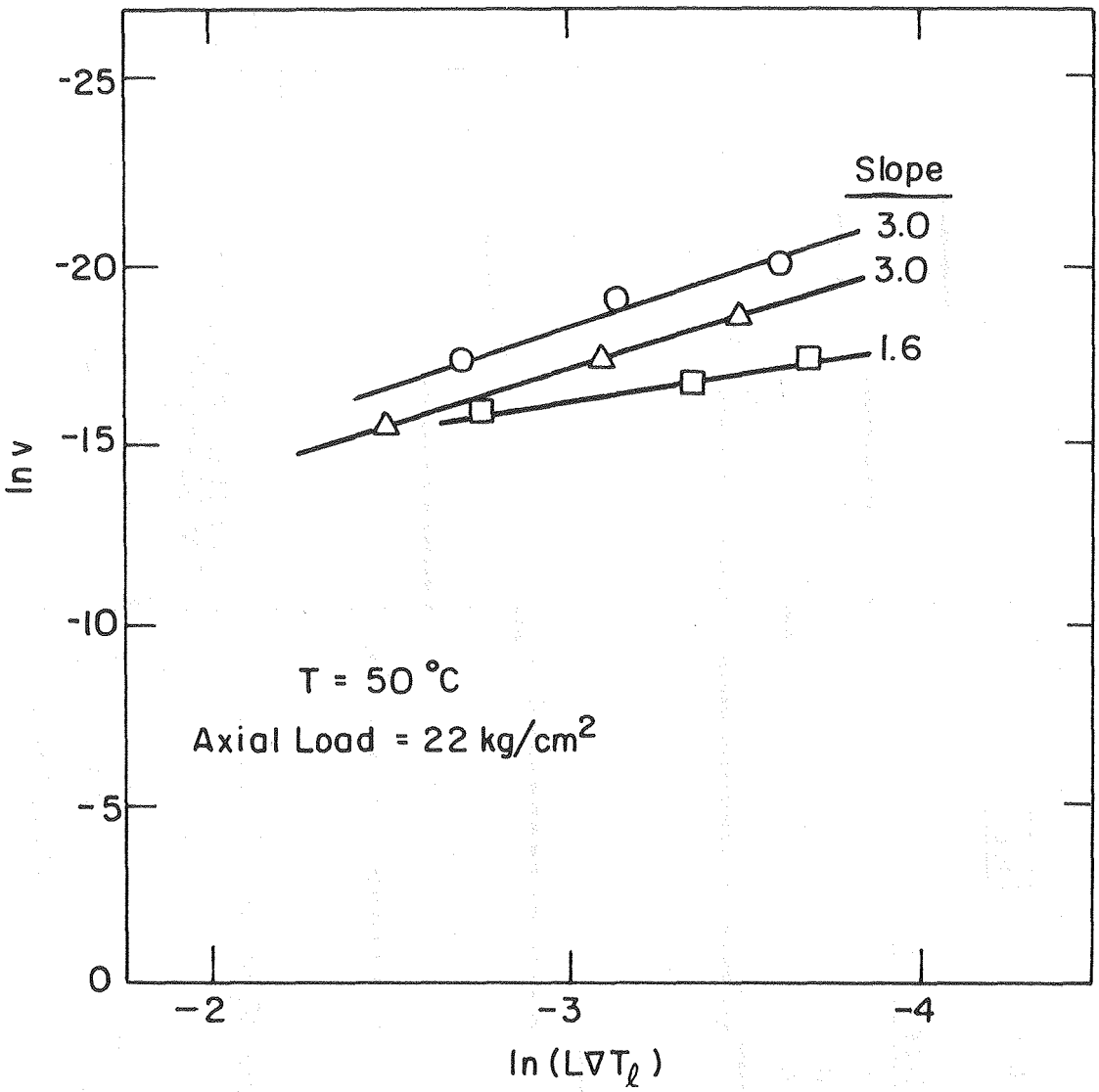

Fig. 14

XBL808-5648

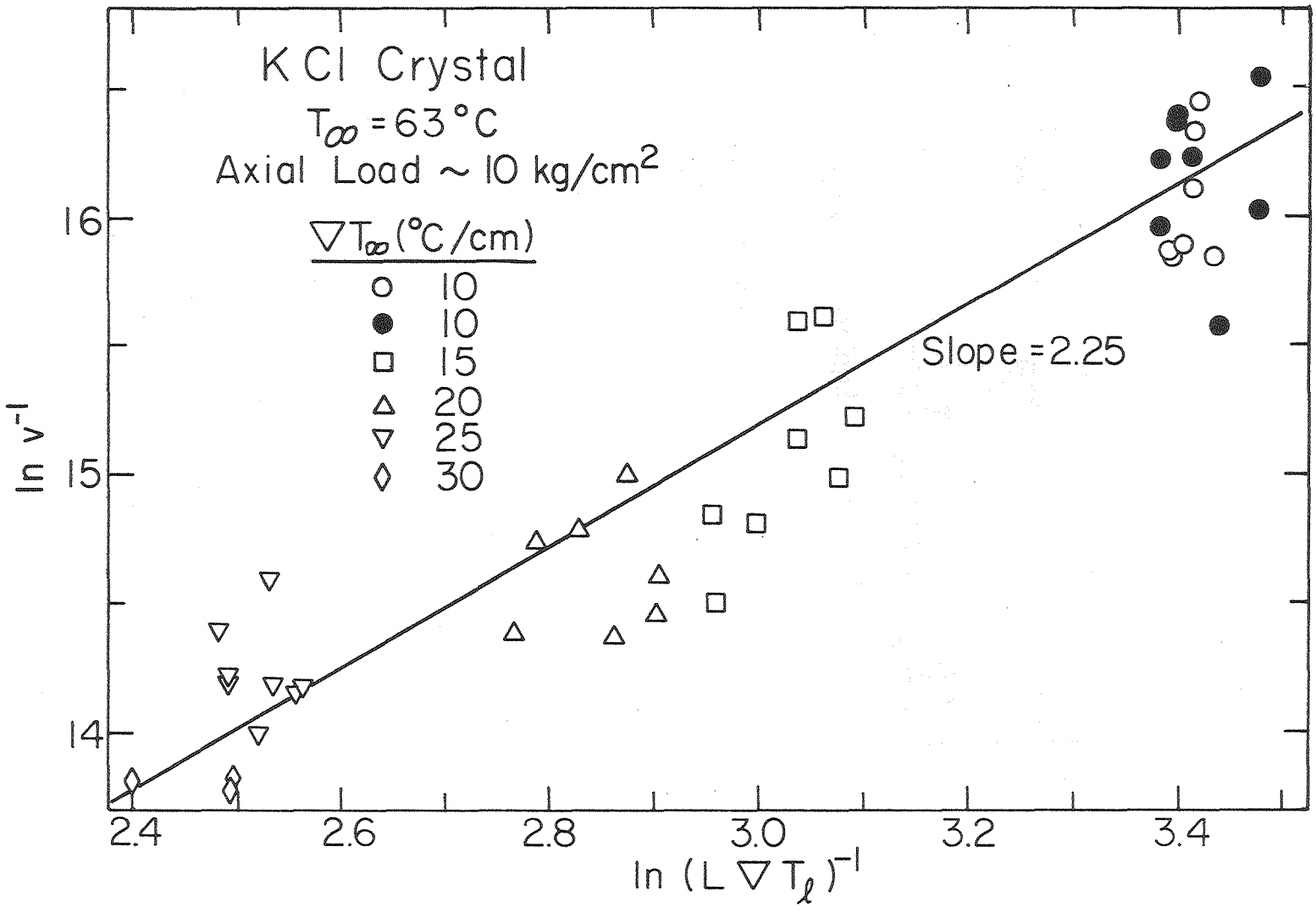

X BL 809-5915

Fig. 15

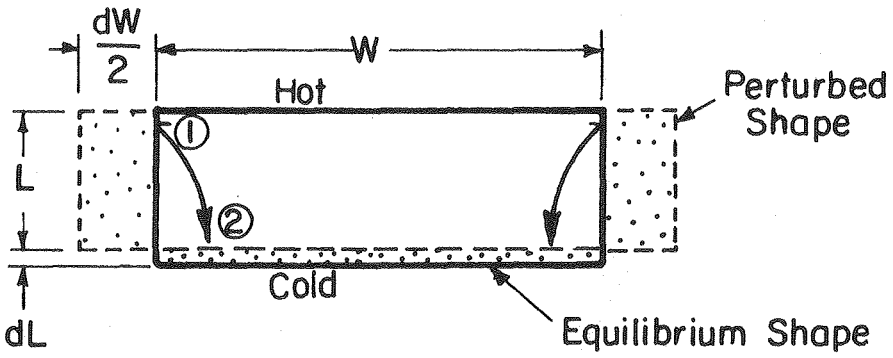

XBL811-5100

Fig. A-1